NOTES AND CORRESPONDENCE

On Estimating Wind Velocity Using an Upward-Looking ADCP

GEORGE O. MARMORINO

Remote Sensing Division, Naval Research Laboratory, Washington, D.C.

ZACHARIAH R. HALLOCK

Oceanography Division, Naval Research Laboratory, Stennis Space Center, Mississippi

8 July 1999 and 31 July 2000

ABSTRACT

A new set of measurements made using an upward-looking broadband acoustic Doppler current profiler (ADCP) is analyzed for ''surface velocity,'' which previous investigations suggest is related to wind velocity. In the present case, use of a shallow instrument depth and 1-m-depth resolution are shown to yield both a surface return, identified by a maximum in backscatter intensity (similar to previous studies), and a subsequent return that corresponds to a maximum in speed. These returns have speeds (measured relative to the 2-m-depth current) that increase to a peak of 0.7–0.8 m s^{-1} at a wind speed of 4–5 m s^{-1} and decrease for higher wind speeds, a behavior similar to that found by Nakajima et al., who made ADCP measurements using the same incidence angle (20°) as in the present study. A new finding is that the return having maximum speed yields a direction that better approximates the wind direction (a mean difference of about 5°) over the range of wind speeds sampled (up to 17 m s^{-1}). Suggestions are made for future investigations.

1. Introduction

The possibility of extracting information useful for determining surface winds from an upward-looking acoustic Doppler current profiler (ADCP) deployed safely beneath the sea surface was first demonstrated by Schott (1989). He found in data collected in the Gulf of Lions that the direction of the acoustic Doppler velocity associated with the surface range bin (i.e., the range bin having maximum backscatter signal in an individual profile) was correlated with the wind direction as measured by a nearby research vessel. Schott also found, however, that the magnitude of this ADCP ''surface velocity'' was apparently uncorrelated with wind speed, as he found surface speeds of 0.5 m s^{-1} and more under both low and high winds. Because these high values of surface speed greatly exceeded the expected near-surface current, Schott proposed that Bragg scattering modulated by longer surface gravity waves (analogous to radar composite scattering) was primarily responsible for the surface Doppler shifts he measured. (In Bragg scattering, the acoustic wave incident on the surface selects out of the spectral distribution of surface wavelengths those leading to constructive, or resonant, interference; for common ADCP frequencies, the Bragg-resonant waves are a few centimeters in wavelength.)

Subsequent studies have tended to confirm a relationship between ADCP surface and wind directions, but the behavior of surface speed versus wind speed is considerably less clear, as illustrated in Fig. 1. Data collected in the equatorial Pacific by Nakajima et al. (1995) show surface speeds exceeding 1 m s^{-1} for winds of 2–8 m s^{-1}; only at very low and high wind speeds do surface speeds approach the wind-drift current (shown as 3% of the wind speed). Nakajima et al.'s results are thus consistent with the generally high surface speeds found by Schott; similarly, high surface speeds were observed by Visbeck and Fischer (1995; their Fig. 9d) under ice-free conditions. Figure 1 also shows the results of Zedel et al. (1996) for their Ocean Storms dataset collected in the North Pacific. In contradistinction to the Nakajima et al. observations, Zedel et al. found significantly smaller surface velocities over the same range of wind speeds. Zedel et al. attribute their results to scattering from a layer of bubbles distributed just beneath the surface at low wind speeds but deepening at high wind speed to give an effectively

Corresponding author address: Dr. George O. Marmorino, Remote Sensing Division, Code 7250, Naval Research Laboratory, Washington, DC 20375-5351.
E-mail: marmorino@nrl.navy.mil

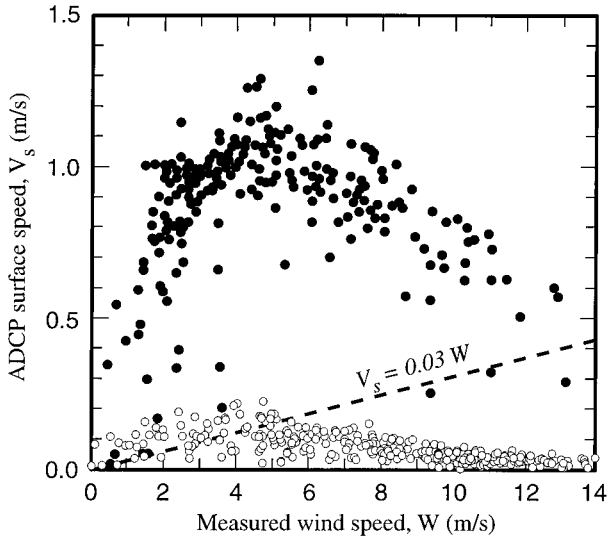

FIG. 1. ADCP-derived surface speed vs measured wind speed as determined in two previous investigations. Filled circles: Nakajima et al.'s (1995, their Fig. 6a) equatorial Pacific dataset. Unfilled circles: Zedel et al.'s (1996, their Fig. 2), North Pacific dataset.

deeper weighting of the ADCP scattering volume. This seemed consistent with an observed Ekman-like veering of their surface velocity vector as the wind speed increased. Thus, the disparity shown in Fig. 1 appears to arise from real differences in scattering physics. Given the range of results and differing explanations, one may conclude that the meaning of the ADCP surface velocity vector is not clear nor is its possible relationship to the wind vector.

This note presents an analysis of a new dataset, which may offer some insight into these issues. Data were collected using ADCPs mounted on the bottom in shallow water, which differs from deep-sea moorings used in the previous work. Also, a vertical bin size of 1 m was used, which is 4–10 times smaller than used in the previous studies. It will be shown that this higher vertical resolution allows a separation of the high-backscatter surface return from a subsequent return having generally the maximum speed in the profile. An investigation of the speed and directional characteristics associated with these two signals is the focus of this paper. The major result is that the velocity vector associated with the maximum-speed return is better correlated with the wind vector and provides an improved estimate of the local wind direction.

2. Approach

a. Background

The measurements were made during the third Chesapeake Bay Outflow Plume Experiment (COPE-3), which was conducted from early October through November 1997 (e.g., Vesecky et al. 1998; Marmorino et al. 1999). A total of six moorings were deployed across the inner shelf in water depths of 10–18 m to investigate the response of the plume to variable wind forcing under the relatively low freshwater discharge conditions typical of the fall. Analysis in the present paper is restricted to a single mooring, A4 (18-m depth), at which data were collected from 5 October to 10 November 1997. A separate analysis of the surface-velocity data from a second mooring, A3, having a similar water depth (17.2 m) and record length, showed statistically identical behavior to that reported. Mooring A4 was located at 36.87°N, 75.78°W, about 22 km from the mouth of the Chesapeake Bay. Limited hydrographic measurements suggest that the water stratification at the mooring site was weak except under southerly, upwelling-favorable winds, when less-dense water from the bay was advected offshore. The approximate tidal range near the mooring is about 1 m.

Auxilliary environmental data are available from a National Data Buoy Center station on the Chesapeake Light Tower, located at 36.90°N, 75.71°W and about 5.5 km northeast of mooring A4. In particular, winds were measured at tower height (43 m above sea level) at 10-min intervals, and the significant wave height was determined at hourly intervals.

b. Instrumentation

The measurements were made using a 307.2-kHz broadband ''Workhorse'' ADCP, manufactured by RD Instruments (RDI). This unit uses four acoustic beams, each having an incidence angle $\theta = 20°$ and a beamwidth of 3.8°. (The beamwidth is given by the acoustic wavelength $\lambda_{adcp} = 0.488$ cm divided by the transducer diameter of 7.3 cm.) The Bragg wavelength $\lambda_B = \lambda_{adcp}/2 \sin\theta = 0.73$ cm. The Bragg waves have a phase velocity of about 0.27 m s^{-1}. The instruments were deployed on the bottom, which eliminated wave-induced instrument motion. There were, however, two instances when the instrument mountings apparently shifted because of strong near-bottom currents. These shifts slightly altered the instrument attitude and heading but had no apparent effect on the quality of the measurements. A vertical bin size of 1 m was used, and the instrument was programmed to collect data over a greater number of bins than necessary to ensure that currents would be measured over the fullest extent possible of the water column. This resulted in the surface return data that are the focus of the present study. Thus, data were collected at approximate bin depths of 14 m, . . . , 1 m, 0 m, −1 m, . . . , and −4 m, where the 0-m bin is expected to contain the surface return, on the average, and negative values indicate returns subsequent to the surface return. (The accuracy of the mean bin depths is the order of 0.5 m.) Given the instrument beamwidth, beam angle, and instrument depth H, the vertical extent of the surface return can be estimated by geometrical considerations as 0.054 H or about 1.0 m (Visbeck and Fischer 1995). Surface waves and depth-penetrating bubble clouds will

TABLE 1. Comparison of some previous investigations with the present study. Parameters are acoustic frequency, f_0; instrument depth (distance from surface), z; vertical bin size, Δz; incidence angle, θ; and Bragg wavelength, λ_B. The parameters on line 3 refer to Zedel et al.'s (1996) ''Ocean Storms'' dataset.

Investigation	f_0 (kHz)	z (m)	Δz (m)	θ (°)	λ_B (cm)
1. Schott (1989)	150	553	9	20	1.5
2. Nakajima et al. (1995)	150	172	9	20	1.5
3. Zedel et al. (1996)	150	110	4	30	1.0
4. Present study	300	18	1	20	0.7

tend to broaden this, so the surface return might be spread over more than one bin or occur in different bins at different times. The tidally changing water depth will produce a similar effect (but see section 3b).

The sampling scheme used was a 1-min burst of 120 samples, which was repeated at 5-min intervals. Burst sampling was used to minimize aliasing of the current measurement by surface gravity waves. (Because of the necessarily long deployment to study the outflow plume, individual ping data could not be recorded.) Other than this choice, the setup of the instruments followed the default options under RDI's ''PLAN'' software (version 1.40). Velocity data from each sample were resolved into east and north components, then averaged over the burst. Averaged values of backscatter intensity and correlation magnitude were recorded separately for each beam. The backscatter data can be used to identify those returns coming from the surface, to correlate against wind speed, and potentially to identify returns from sidelobes or other effects (e.g., Schott 1989). Intensity units (or counts) vary from 0 to 255; counts below 190 are proportional to backscatter intensity as measured in decibels, but the relationship for counts above 190 is a poorly known nonlinear one (RDI 1999, personal communication). Relative to the main lobe, the first ($\pm 5°$) sidelobe is depressed by 18 dB; thus, a sidelobe return from the same structure sampled by the main beam would appear in the data with an intensity value lower by at most 18 counts. Not having calibrated intensity data is a deficiency of the present study. The correlation magnitude (counts divided by 255) is a measure of the pulse-to-pulse correlation in a ping for each depth bin. Examination of each beam's intensity and correlation data showed qualitatively identical behavior. Therefore, we chose to show in this paper only data from beam 3, which was oriented toward 13.6°T.

The major differences in instrumentation and deployment between the present study and those mentioned in the introduction are summarized in Table 1. Previous studies used deep-sea moorings with the ADCP at a depth of 100 m or more. The sea surface area insonified by each acoustic beam was thus several tens of meters in diameter for an individual ping. In the present study, the corresponding dimension is about 1.4 m. Previous studies used vertical bin sizes of 4–9 m as compared to the present 1-m bins. Also, the present study has the smallest Bragg wavelength. A final difference is that previous studies used narrowband ADCPs, while we used a broadband instrument.

c. Computation of relative current and other processing details

To extract more effectively the wind-driven motion from the surface velocity measurement, previous investigators have suggested first subtracting the background current. Nakajima et al. (1995) define the ''wind-induced surface velocity'' (WSV) as the vector difference between the surface velocity and a near-surface reference velocity measured in the depth bin just below the sidelobe contaminated layer. This layer, over which data are expected to be contaminated by sidelobe direct reflections from the surface, has a depth range $L = H(1 - \cos\theta)$, where H is the transducer depth. In Nakajima et al.'s dataset, $L = 10$ m, and their WSV values (referenced to the current at 20 m) are replotted in our Fig. 1. Essentially the same procedure is recommended by Zedel et al. (1996), who define a surface drift velocity $\mathbf{V}_{\text{drift}} = \mathbf{V}_{\text{surface}} - \mathbf{V}_{\text{reference}}$, where $\mathbf{V}_{\text{reference}}$ is the current averaged over a suitably chosen depth range. The Zedel et al. values (Fig. 1) assume $\mathbf{V}_{\text{reference}} = 0$, as the background current in their Ocean Storms dataset was judged by them to be weak enough to be ignored. (They do, however, report directional characteristics of $\mathbf{V}_{\text{drift}}$ in their paper, where the reference velocity is at 16-m depth.) Following Nakajima et al., we will use a reference velocity from just below the sidelobe contaminated layer. In our case, $H = 18$ m and $\theta = 20°$, so that $L = 1.1$ m; thus, the reference bin will be at 2-m depth and the ADCP velocity vectors analyzed in the next section are relative to the 2-m-depth velocity vector.

In addition, to reduce high-frequency sample variability, all data were 3-h lowpassed and then subsampled at 0.5-h intervals. Also, to reduce scatter in the results, data have been averaged in 0.5 m s^{-1} bins of wind speed. Current and wind directions are measured counterclockwise from east, where wind direction refers to the direction toward which the air flows (in analogy with the current direction).

3. Results

a. Mean profiles

Figure 2 shows profiles of backscatter intensity (beam 3), speed, and correlation (beam 3) averaged over the entire dataset. The intensity profile (Fig. 2a) peaks at 0-m depth, which is the expected surface bin. As in previous work, returns from this bin are assumed to be caused primarily by the direct surface (or near surface) return of the main-lobe energy. Signals recorded after this surface return must obviously derive through some other mechanism. These subsequent returns have intensities that mirror the behavior at deeper bins; this be-

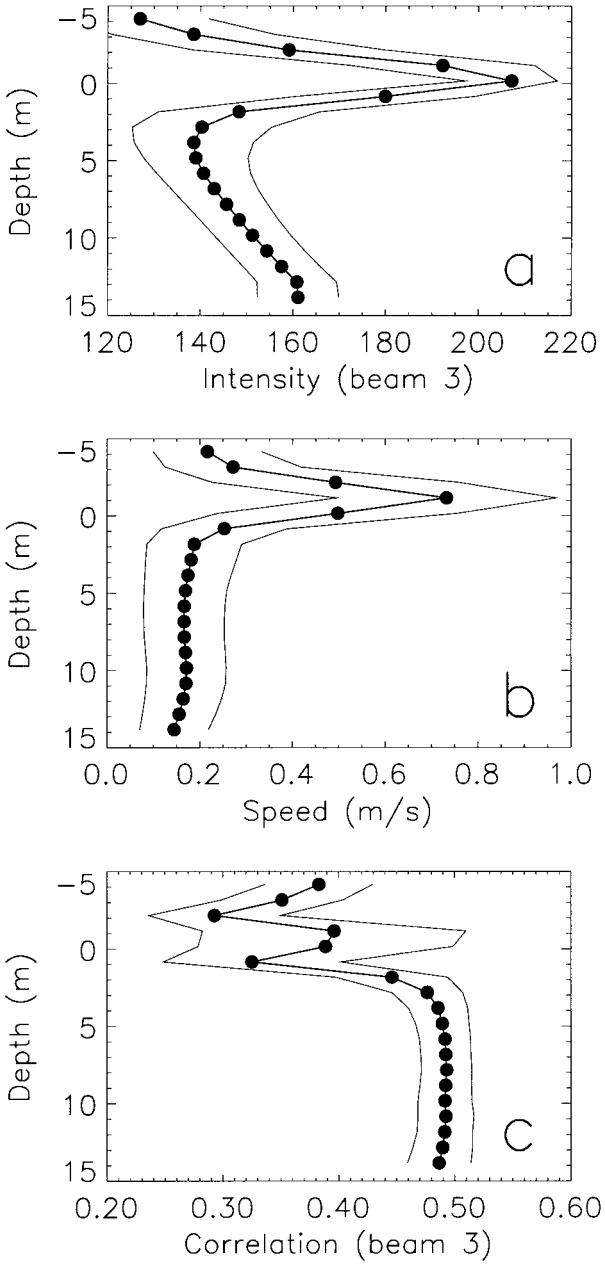

FIG. 2. Mean profile of (a) backscatter intensity, (b) speed, and (c) pulse-to-pulse-correlation values. Profiles in (a) and (c) are for beam 3 but are representative of results for the other three beams. Negative depths correspond to returns subsequent to the surface return (i.e., the return from the mean 0-m depth bin). Filled circles are the means; curves show ± one standard deviation.

havior is similar to that found in the intensity profile measured by Visbeck and Fischer (1995) and which they attributed to the influence of sidelobes. Of particular interest is the very next return (from the −1-m bin) because it has the largest speed in the mean profile (Fig. 2b). This value (about 0.73 m s^{-1}) is 50% larger than the speed at the 0-m bin and about four times the mean speed in the deeper part of the water column. The mean correlation profile is shown in Fig. 2c. These values signify the degree to which an acoustic pulse scatters coherently from the same collection of scatterers in a given range bin. High correlations (about 0.50) apply over most of the water column but decrease abruptly near the surface, reaching a value of only 0.33 at 1-m depth, which corresponds to the expected depth of the sidelobe contamination layer. The correlation increases to about 0.39 at the 0- and −1-m bins; this being less than 0.5 indicates that these returns also have, on average, some loss of correlation.

b. Variations with wind speed

In order to study variability within the dataset, values of intensity, velocity, and correlation were extracted from each individual profile (5-min samples) at the bins having the maximum speed (S_{max}) and the maximum intensity (I_{max}). We denote as $\mathbf{V}_{S\max}$ and $\mathbf{V}_{I\max}$ the velocity vectors corresponding to the S_{max} and I_{max} returns. These vectors $\mathbf{V}_{S\max}$ and $\mathbf{V}_{I\max}$ and their associated speeds, S_{max} and $S_{I\max}$, are taken to be relative to velocity at 2-m depth (section 2c). Note that these values are not associated with fixed depth bins but, as in the mean profile, the S_{max} value generally occurred one bin after the I_{max} value. The depths of these returns varied systematically over the tidal cycle, so any effect on the results of tidally induced water-level change was diminished. A related effect, which could not be addressed directly, is any large wave-induced change in surface height during a burst average. This will lead to some mixing of these effects between bins as discussed in section 2b.

Figure 3a and 3b show the variation of S_{max} and $S_{I\max}$ with wind speed. For reference, the expected speed of the wind-drift current (calculated as 3% of the wind speed) is also plotted. Both S_{max} and $S_{I\max}$ increase steeply as the wind increases and reach peaks of about 0.8 and 0.7 m s^{-1} at a wind speed of 4–5 m s^{-1}. (The rate of increase is about 0.25 and 0.20.) This behavior is most similar to that found by Nakajima et al. (1995), but a peak also occurs at about this same range of wind speeds in the Zedel et al. (1996) study (Fig. 1). Except at the lowest wind speeds, the values of S_{max} and $S_{I\max}$ are too large to be explained by wind drift plus first-order Bragg scattering. For wind speeds greater than about 5 m s^{-1}, the $S_{I\max}$ data decrease, crossing the wind-drift line at a wind speed of 11 m s^{-1} and tending toward 0 m s^{-1} at higher wind speeds. The S_{max} data, on the other hand, remain higher than the wind-drift current over the entire wind speed range.

Figure 3c shows the corresponding plot of I_{max}. Similar to the plots of speed, low intensity values occur at low wind speed. This behavior (and the range of I_{max} intensity values) is similar to that found by Nakajima et al. The leveling off of I_{max} for wind speeds in excess of 5 m s^{-1} is similar to incoherent acoustic measurements made by Nutzel and Herwig (1995; their Fig. 9),

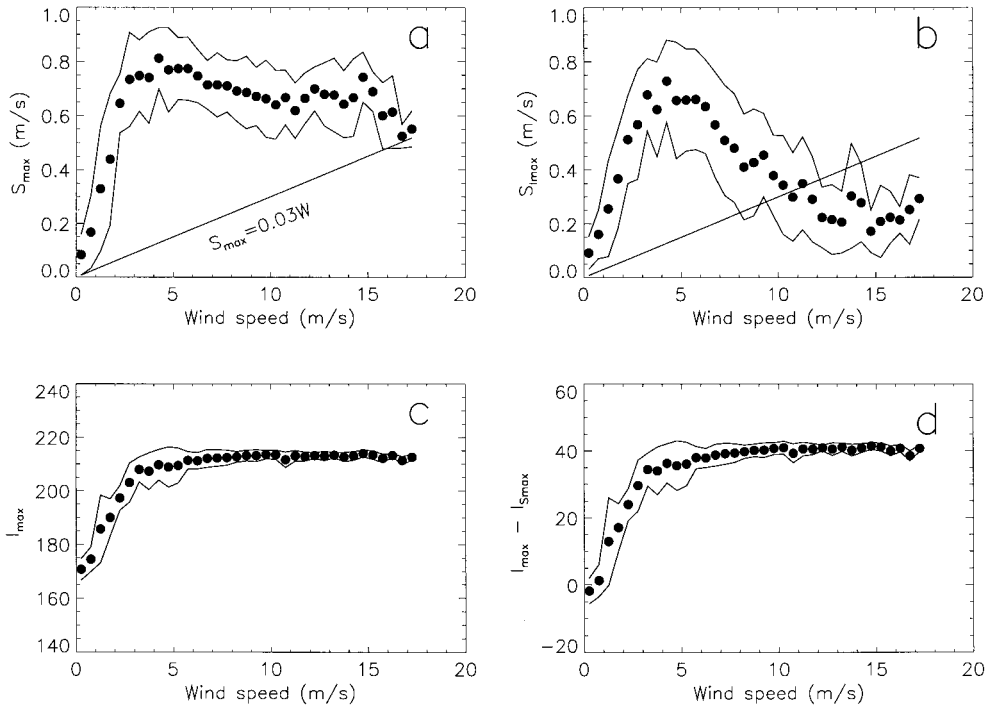

FIG. 3. Variations with wind speed of (a) S_{max}, (b) S_{Imax}, (c) I_{max}, and (d) $I_{max} - I_{Smax}$. Filled circles are the means; curves show ± one standard deviation. Here S_{max} and I_{Smax} ($S_{Imax}$and I_{max}) are speed and intensity at the range bin having the maximum speed (intensity). Speeds are measured relative to the current at 2-m depth.

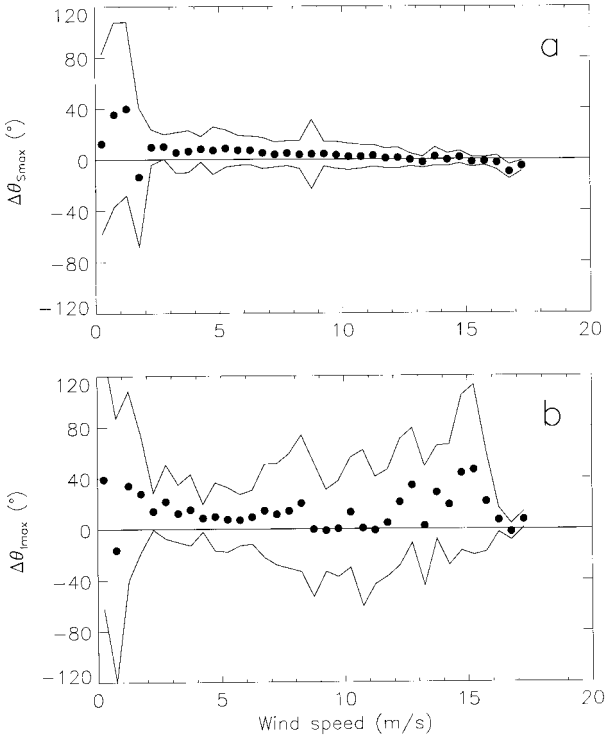

FIG. 4. Difference in direction between the wind and (a) $\mathbf{V}_{Smax}$ and (b) $\mathbf{V}_{Imax}$. In both (a) and (b) the velocity vector is relative to the current at 2-m depth. A negative value of $\Delta\theta$ means the relative current vector lies to the right of the wind vector.

which show saturation of the acoustic return occurring at a wind speed of about 5 m s^{-1} for frequencies greater than 50 kHz (and an incidence angle of 45°). Figure 3d shows the difference in intensity between the I_{max} and S_{max} returns. A difference of about 40 counts is found for wind speeds greater than 5 m s^{-1}, and even at higher wind speeds it was found that S_{max} still tends to occur one bin later than I_{max}. An examination was also made of the behavior of the pulse-to-pulse correlation with wind speed (not shown). At both the S_{max} and I_{max} bins, highest values (≈0.5) occur for the lowest wind speeds, but otherwise the correlation values showed little trend with wind speed. Thus, the scattering appears to be uniformly less coherent over moderate to high wind speeds.

The directional difference $\Delta\theta$ between each of the ADCP velocity vectors and the wind vector is plotted against wind speed in Fig. 4. When $\mathbf{V}_{Smax}$ is used (Fig. 4a), the $\Delta\theta$ values show a positive bias of about 7° for moderate wind speeds (3–7 m s^{-1}) then a trend of gradually decreasing values over higher wind speeds. At the lowest wind speeds, both $\Delta\theta$ and its standard deviation $\sigma_{\Delta\theta}$ are much increased. This may be the result of the wind direction being poorly resolved at wind speeds less than 2 m s^{-1}, or the ADCP is responding to surface structure associated with waves that are not in equilibrium with the local wind. Ignoring these lowest wind speeds, $\sigma_{\Delta\theta} \approx 12°$ for the $\mathbf{V}_{Smax}$ case for moderate wind speeds, decreasing to about half this above 12 m s^{-1}. In the case of $\mathbf{V}_{Imax}$ (Fig. 4b), the behavior of $\Delta\theta$ is

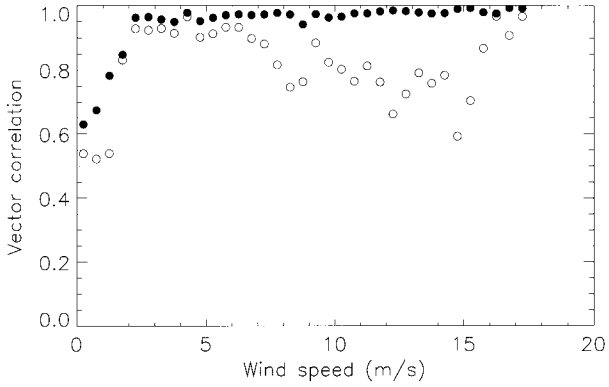

FIG. 5. Vector correlation between wind and $\mathbf{V}_{S\max}$ (filled circles) and $\mathbf{V}_{I\max}$ (unfilled circles).

similar for wind speeds less than 6 m s^{-1}, but there is so much more variability at higher wind speeds ($\sigma_{\Delta\theta} \approx 40°$) that it is not possible to discern if there is any trend with wind speed.

To see if the trend in $\Delta\theta_{S\max}$ values is with wind speed alone or whether some other variable is involved, we reexamined the data for evidence of an effect related to significant wave height (section 2a). For wind speeds in the range of 2–9 m s^{-1}, the dataset was first divided into roughly equal parts, one having wave heights less than 0.8 m and the other greater than 0.8 m. New plots of $\Delta\theta_{S\max}$ (not shown) indicate that the higher-height population has uniformly smaller values of $\Delta\theta$ (about 4°) compared to the smaller-height population (about 9°). (There was no similar effect discernable in the case of $\Delta\theta_{I\max}$; nor were there clear differences in the behavior of either $S_{\max}$ or $S_{I\max}$ with wind speed). This suggests that characteristics of the surface wave field, such as enhanced surface slopes or increased wave breaking, are affecting the $S_{\max}$ return and improving the estimation of local wind direction. Also, this provides some evidence that a varying sea surface height during a burst sample is not causing any more of a problem at high versus low sea states.

c. Vector relationships

In order to quantify the relationships between the time series of $\mathbf{V}_{S\max}$ and $\mathbf{V}_{I\max}$ versus the wind vector, we computed a vector correlation coefficient, the magnitude of which provides an overall measure of correlation between the vectors (Kundu 1976). In the case of $\mathbf{V}_{S\max}$ (Fig. 5; filled circles), values of the correlation exceed 0.95 except at wind speeds less than 2 m s^{-1}. The behavior of relative phase angle between the vectors (not shown) yields a result similar to the plot of $\Delta\theta$ in Fig. 4a. In the case of $\mathbf{V}_{I\max}$ (Fig. 5; unfilled circles), the correlation is significantly lower for wind speeds greater than about 7 m s^{-1} and, correspondingly, there is more variability in the phase angle (similar to Fig. 4b).

In order to judge the effect of the higher values of correlation seen in Fig. 5, we calculated a linear regression of the wind vector on $\mathbf{V}_{S\max}$ and used the result to synthesize or create a ''predicted'' wind vector time series. The predicted wind is given by $\mathbf{W} = a\mathbf{V}_{S\max} + b$, where a and b are complex regression coefficients. The predicted and observed winds are compared in Fig. 6 for the special case where b is set equal to zero so that zero velocity produces a zero wind vector; in this case, the coefficient a had a magnitude of 10.2 and a phase angle of $-4°$. (A separate calculation with no constraint on b gave very similar results.) The predicted wind speeds do not in general show very good agreement with the observed wind speeds. An exception is the tendency for very low values of predicted and observed wind speed to occur together. Gross underestimation of the wind speed occurs at several times, most noticeably on day 292, which was the period of strongest observed winds. The comparison of predicted and observed wind direction, on the other hand, is strikingly good. Notice in particular the many instances of agreement over rather abrupt changes in wind direction such as on days 288 and 311. It is therefore the directional agreement that primarily accounts for the high vector correlation.

Some improvement in the predicted wind speed could likely be made by doing a multiple regression of the wind speed on ADCP speed and intensity. The reasoning here is that our results (Figs. 3a, b) and those of Nakajima et al. (1995) do show a functional relationship between the ADCP speed and the wind speed. This includes a rapid rise to a peak value of the order of 1 m s^{-1} at a wind speed of 4–5 m s^{-1} and then a more gradual decrease over higher wind speeds. The problem is that this relationship is a nonlinear and multivalued one; however, this can be circumvented by adding a constraint based upon the behavior of the surface backscatter intensity with wind speed. For example, if $I_{\max} < 210$ counts (Fig. 3c), then use the low-wind trend in the plot of $S_{I\max}$ versus wind speed (Fig. 3b) to estimate the wind speed; otherwise, use a fit to the high-wind part of Fig. 3b to estimate the wind speed. (Figure 3b is used as it shows a stronger overall dependence on wind speed.) In such an approach, the details of which we do not pursue, the $I_{\max}$ return would thus yield the wind speed estimate, while the $S_{\max}$ return would yield the estimate of wind direction.

4. Discussion

While there are many experimental differences between the present study and previous ones, the results are nevertheless similar in several respects. One similarity is the occurrence of a peak in the ADCP ''surface'' speed at a wind speed of 4–5 m s^{-1}. As suggested by Nakajima et al. (1995) and Zedel et al. (1996), it may be at this range in wind speed that scattering from subsurface bubbles becomes comparable to scattering from surface structure (see below). Another similar finding

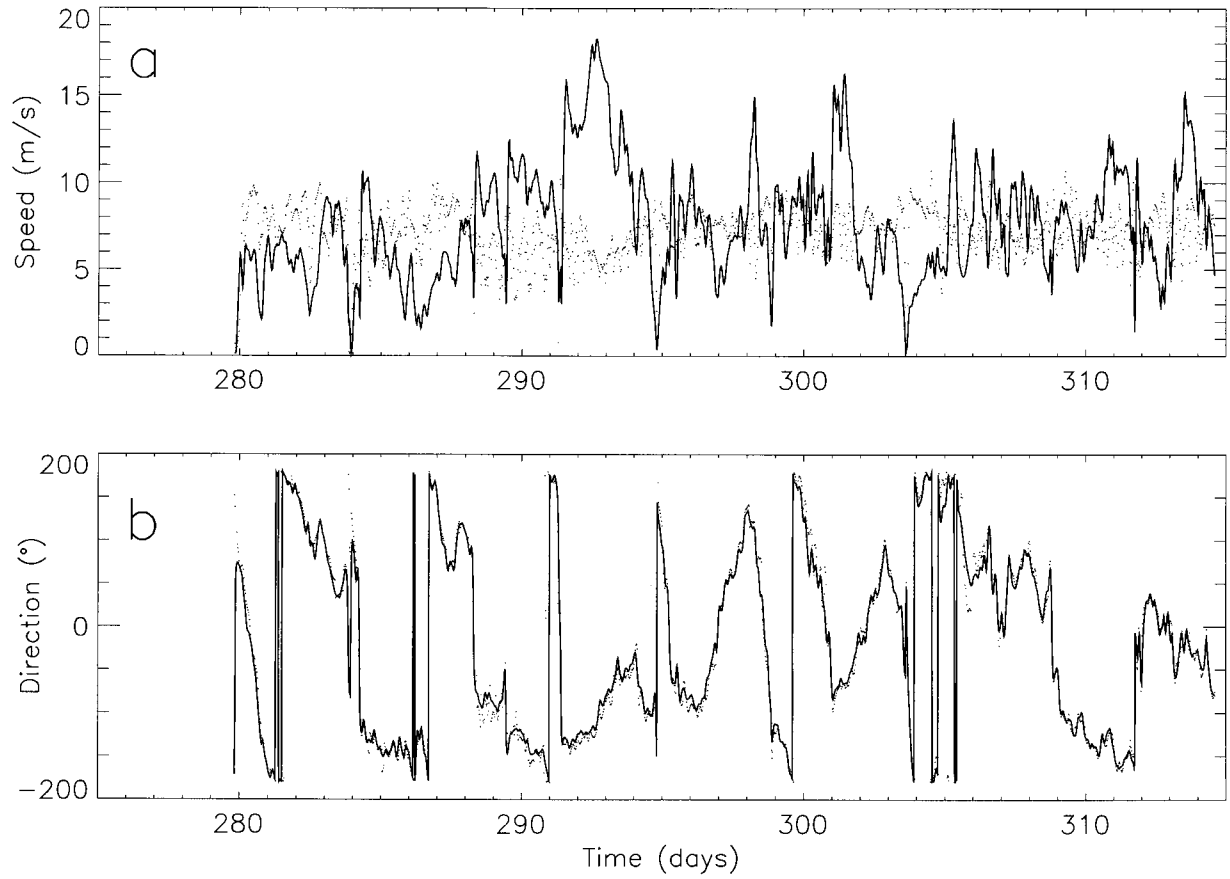

FIG. 6. Predicted (dots) vs observed wind speed and wind direction. The predicted wind vector was calculated from the linear regression $\mathbf{W} = a\mathbf{V}_{S\max}$, where a is a complex regression coefficient.

is a high degree of correlation between the direction of the surface and wind vectors. Schott (1989), who used 12-h averages and wind speeds >3 m s^{-1}, found a correlation coefficient of 0.98. He also found that the surface velocity vector was on average rotated 5° to the right of the wind (i.e., in a sense consistent with Ekman dynamics). Zedel et al., who used 24-h averages and wind speeds >2 m s^{-1}, found a correlation coefficient of 0.95 between wind direction and the direction of their $\mathbf{V}_{\text{drift}}$ velocity vector (section 2c). This vector was rotated on average 6° (±24°) to the left of the wind but, as $\mathbf{V}_{\text{drift}}$ is a relative current, the significance of the rotation angle is not clear. (However, the absolute surface velocity vector in their study, too, was directed to the right of the wind vector by about 12°, on average.) In the present work, use of 1-m bins allowed a separation of the near-surface data into a high-intensity ($I_{\max}$) surface return and a subsequent (generally the very next bin) low-intensity but maximum-speed ($S_{\max}$) return. When we compare values of 3-h lowpassed wind direction to the direction of the maximum-speed velocity vector $\mathbf{V}_{S\max}$ (relative to the current at 2-m depth), the mean correlation coefficient was 0.97 and the relative velocity vector was rotated on average about 5° to the left of the wind (similar to the Zedel et al. result). Our results based on $\mathbf{V}_{S\max}$ are superior to those using $\mathbf{V}_{I\max}$, which we identify as analogous to the surface return used by the previous investigators.

The major difference among the ADCP studies conducted so far appears to be the absence of high values of surface speed in the Zedel et al. study. This difference may arise from either scattering physics or ADCP processing. The physical explanation proposed by Schott for the high surface speeds he measured is wave-related surface scattering. It is expected that surface scattering will dominate the acoustic backscatter for very small incidence angles, while scattering from bubbles will dominate for large angles (Dahl et al. 1997). Thus there should be more of a contribution from surface scattering in the ADCP measurements made at 20° incidence than in Zedel et al.'s made at 30°. Surface scattering can be modeled as for the analogous radar problem, using a composite model that includes tilted Bragg waves and specular scatter. In the case of tilted-Bragg scattering, a high-backscatter weighting occurs at the phase of the wind-generated waves tilted toward an acoustic beam and biases the time-averaged Doppler measurement toward the corresponding wave orbital velocity. In spec-

ular scattering, a tilted wave facet or parasitic structure trapped to the forward face of a wave biases the measurement toward the wave's phase velocity. Thus, surface-scattering effects can produce current estimates that are much larger than the actual mean surface current (plus the motion of the resonant Bragg waves). Thompson et al. (1991) clearly show this for Ku-band radar measurements ($\lambda_B \approx 3$ cm). Wave-related effects in the ADCP surface measurements might therefore yield a speed more proportional to a wind-driven wave velocity than the wind-induced current; however, the ADCP-measured direction may still be a good estimator of the wind direction. Such wave-related biases should decrease as scattering from near-surface bubbles becomes dominant at the higher wind speeds. The wind speed at which this transition occurs varies with acoustic frequency and incidence angle; for example, at 50 kHz and 45° incidence the transition wind speed appears to be about 5 m s^{-1} (Nutzel and Herwig 1995; Dahl et al. 1997).

To explore a possible ADCP-processing explanation for the high surface speeds, consider the following. The S_{max} return most likely arises from scattering of a sidelobe or multiple scattering of the main beam. Because this return occurs immediately after the surface return and has a high directional correlation with the wind, we postulate that the scattering is near-surface and occurs along a horizontal path. The total Doppler shift will then be most sensitive to the local horizontal velocity (either wind-drift current or wave related). However, the ADCP processes all Doppler shifts as though they arise from a projection of the velocity vector onto the beam axis. In a simple two-beam solution, the ADCP would thus yield through such an effect an apparent horizontal velocity that is a factor of $1/\sin\theta$ larger than the actual horizontal velocity. For $\theta = 20°$, this factor is nearly 3 (2.92). In effect, multiple scattering could lead to Doppler shifts from real horizontal velocities that are directionally misinterpreted by the ADCP. Such effects may become important at the higher wind speeds as more acoustic energy is scattered sideways from an increasingly rough sea surface (Schott 1989). All returns subsequent to the sidelobe contamination layer (section 2c) could have some contribution from such multiple scattering effects. Note that for the 30° incidence angle used by Zedel et al. the factor $1/\sin\theta = 2.0$, which would indeed yield less of an effect in their case; however, it is also possible some other detail of the ADCP processing is involved.

In conclusion, our work has suggested that ADCP measurements having high resolution in depth may be of some use in estimating characteristics of the surface wind. The major result is the discovery of a $\mathbf{V}_{Smax}$ signal that, compared with the surface return in our work, is more highly correlated with the wind vector even at the highest wind speeds sampled (17 m s^{-1}) and better estimates the wind direction (a mean difference of about 5°). Also, based on the similarity of our results to those of Nakajima et al., we have suggested a scheme for improving the estimation of wind speed. In our opinion, more work is needed on this subject. In future study, the investigator should strive to record single-ping radial velocity data and calibrated intensity data for each beam. Also, it would be useful to collect the ADCP data in conjunction with radar measurements having the same Bragg wavelength, as few comparative studies have been made (e.g., Dahl et al. 1997). This would allow differentiating between different kinds of surface scattering (specular and tilted-Bragg) and scattering from bubbles and hence between wave- and current-related effects.

Acknowledgments. This is a contribution to the Physics of Coastal Remote Sensing Accelerated Research Initiative (PE–61153N), funded by the Office of Naval Research and managed at the Naval Research Laboratory by Dr. Richard Mied.

This note is dedicated to Dr. Dennis B. Trizna on the occasion of his retirement from the Naval Research Laboratory.

REFERENCES

Dahl, P. H., W. J. Plant, B. Nutzel, A. Schmidt, H. Herwig, and E. A. Terray, 1997: Simultaneous acoustic and microwave backscattering from the sea surface. *J. Acoust. Soc. Amer.*, **101,** 2583–2595.

Kundu, P. K., 1976: Ekman veering observed near the ocean bottom. *J. Phys. Oceanogr.*, **6,** 238–242.

Marmorino, G. O., C. L. Trump, and Z. R. Hallock, 1999: Near-surface current measurements using a ship-deployed ''horizontal'' ADCP. *J. Atmos. Oceanic Technol.*, **16,** 1456–1463.

Nakajima, H., A. Kaneko, and N. Gohda, 1995: Sea surface measurement by a self-contained upward-looking ADCP. *J. Meteor. Soc. Japan,* **73,** 639–643.

Nutzel, B., and H. Herwig, 1995: Wind speed dependence of acoustic backscattering. *J. Geophys. Res.*, **100,** 24 885–24 892.

Schott, F., 1989: Measuring winds from underneath the ocean surface by upward looking acoustic Doppler current profilers. *J. Geophys. Res.*, **94,** 8313–8321.

Thompson, D. R., B. L. Gotwols, and W. C. Keller, 1991: A comparison of Ku-band Doppler measurements at 20° incidence with predictions from a time-dependent scattering model. *J. Geophys. Res.*, **96,** 4947–4955.

Vesecky, J. F., C. C. Teague, J. D. Paduan, D. M. Fernandez, K. Laws, Z. Hallock, and L. A. Meadows, 1998: Observations of air–sea dynamics by multifrequency HF radar and other environmental sensors outside the mouth of the Chesapeake Bay during the COPE-3 experiment of October–November 1997. *Eos, Trans. Amer. Geophys. Union,* **79** (Spring Meeting Suppl.), S 169.

Visbeck, M., and J. Fischer, 1995: Sea surface conditions remotely sensed by upward-looking ADCPs. *J. Atmos. Oceanic Technol.*, **12,** 141–149.

Zedel, L., G. B. Crawford, and L. Gordon, 1996: On the determination of wind direction using an upward looking acoustic Doppler current profiler. *J. Geophys. Res.*, **101,** 12 163–12 176.